AGU PUBLICATIONS

JGR

Journal of Geophysical Research: Space Physics

RESEARCH ARTICLE

10.1002/2017JA024850

Key Points:
- The strong electrostatic standing structures will be formed through the coupling between counter-propagating whistler mode waves
- The wave number of electrostatic standing structure is twice that of whistler mode wave, while its frequency is approximately zero
- The electrostatic standing structures can further be coupled with whistler mode waves to drive high-*k* modes with the triple wave number

Correspondence to:
X. Gao,
gaoxl@mail.ustc.edu.cn

Citation:
Chen, H., Gao, X., Lu, Q., Sun, J., & Wang, S. (2018). Nonlinear evolution of counter-propagating whistler mode waves excited by anisotropic electrons within the equatorial source region: 1-D PIC simulations. *Journal of Geophysical Research: Space Physics*, *123*, 1200–1207. https://doi.org/10.1002/2017JA024850

Received 3 OCT 2017
Accepted 1 FEB 2018
Accepted article online 7 FEB 2018
Published online 19 FEB 2018

Nonlinear Evolution of Counter-Propagating Whistler Mode Waves Excited by Anisotropic Electrons Within the Equatorial Source Region: 1-D PIC Simulations

Huayue Chen[1,2,3], Xinliang Gao[1,2,3], Quanming Lu[1,2], Jicheng Sun[1,2], and Shui Wang[1,2]

[1]CAS Key Laboratory of Geospace Environment, Department of Geophysics and Planetary Science, University of Science and Technology of China, Hefei, China, [2]Collaborative Innovation Center of Astronautical Science and Technology, Harbin, China, [3]State Key Laboratory of Space Weather, Chinese Academy of Sciences, Beijing, China

Abstract Nonlinear physical processes related to whistler mode waves are attracting more and more attention for their significant role in reshaping whistler mode spectra in the Earth's magnetosphere. Using a 1-D particle-in-cell simulation model, we have investigated the nonlinear evolution of parallel counter-propagating whistler mode waves excited by anisotropic electrons within the equatorial source region. In our simulations, after the linear phase of whistler mode instability, the strong electrostatic standing structures along the background magnetic field will be formed, resulting from the coupling between excited counter-propagating whistler mode waves. The wave numbers of electrostatic standing structures are about twice those of whistler mode waves generated by anisotropic hot electrons. Moreover, these electrostatic standing structures can further be coupled with either parallel or antiparallel propagating whistler mode waves to excite high-*k* modes in this plasma system. Compared with excited whistler mode waves, these high-*k* modes typically have 3 times wave number, same frequency, and about 2 orders of magnitude smaller amplitude. Our study may provide a fresh view on the evolution of whistler mode waves within their equatorial source regions in the Earth's magnetosphere.

1. Introduction

Whistler mode waves are intense electromagnetic emissions that occur naturally in the Earth's inner magnetosphere (Burtis & Helliwell, 1969; Gao, Mourenas, et al., 2016; Meredith et al., 2001; Santolík et al., 2003; Tsurutani & Smith, 1974), which are believed to play an important role in regulating electron dynamics in the Van Allen radiation belt (Horne et al., 2003; Horne & Thorne, 1998; Lorentzen et al., 2001). Through resonant wave-particle interactions, whistler mode waves can efficiently accelerate ~100 keV electrons to ~MeV energies during geoactive periods, leading to the rapid enhancement of relativistic electrons in the outer radiation belt (Meredith et al., 2001; Summers et al., 1998; Thorne et al., 2013; Xiao et al., 2014). Furthermore, they are considered to be the contributor of lower-energy (0.1–30 keV) diffuse auroral precipitation in the Earth's atmosphere (Ni et al., 2008, 2011; Nishimura et al., 2013; Thorne et al., 2010), as well as the relativistic (>1 MeV) electron microburst precipitation (Lorentzen et al., 2001). In the Earth's magnetosphere, whistler mode waves usually exhibit as either discrete rising/falling tones or hiss-like emissions in the dynamic spectrogram (Burtis & Helliwell, 1969; Burton & Holzer, 1974; Gao et al., 2014a; Li et al., 2012), which are typically divided in two bands, that is, lower and upper bands, by a power gap around 0.5 f_{ce} (f_{ce} is the equatorial electron cyclotron frequency) (Li et al., 2011; Santolík et al., 2003; Tsurutani & Smith, 1974). Based on observations by Time History of Events and Macroscale Interactions during Substorms satellites, whistler mode waves in lower band usually have smaller wave normal angles (WNA $< 30°$), but there is also a nonnegligible population with very large WNAs (WNA $> 60°$) (Li et al., 2011).

Both observations (Fu et al., 2014; Gao et al., 2014a; Li et al., 2010) and the linear theory (Gary & Karimabadi, 2006; Kennel & Petschek, 1966; Omura et al., 2008; Scharer & Trivelpiece, 1967) have suggested that energetic electrons (~10 keV) with a temperature anisotropy ($T_{\perp e}/T_{\parallel e} > 1$, where $T_{\perp e}$ and $T_{\parallel e}$ are perpendicular and parallel temperatures of electrons with respect to the background magnetic field, respectively) can provide the free energy to excite whistler mode waves in the Earth's magnetosphere. The major source region of whistler mode waves was predicted to locate near the magnetic equator by the linear theory, where the Earth's magnetic field reaches its local minimum (Helliwell, 1967). This has already been confirmed by many

observational works, further showing that their source region just extends to several degrees of magnetic latitude from the magnetic equator (LeDocq et al., 1998; Parrot et al., 2003; Santolík et al., 2003). In the source region, whistler mode waves are typically detected with opposite Poynting flux directions and very small WNAs (Li et al., 2013), which is also supported by the linear theory (Gary & Karimabadi, 2006; Omura et al., 2008) and particle-in-cell (PIC) simulations (Ke et al., 2017).

Nonlinear wave-wave interactions related to whistler mode waves are attracting more and more attention for their important role in reshaping whistler mode spectra in the magnetosphere (Chen et al., 2017; Fu et al., 2017; Gao, Lu, et al., 2016; Gao, Ke, et al., 2017; Gao, Lu, et al., 2017). Using Time History of Events and Macroscale Interactions during Substorms waveform data, Gao, Lu, et al. (2016) have reported two multiband whistler mode events, where upper-band waves are found to be the second harmonic of lower-band waves. Then, they proposed that upper-band waves are excited through the coupling between the electromagnetic and electrostatic components of lower-band whistler waves (i.e., lower band cascade), which could be a potential generation mechanism of upper-band whistler mode waves in the Earth's magnetosphere. Lower band cascade is also confirmed by PIC simulations, which have successfully reproduced those reported multiband whistler waves (Chen et al., 2017; Gao, Ke, et al., 2017). Moreover, two lower-band whistler mode waves are also observed to resonantly interact with each other, leading to the generation of oblique upper-band waves (Gao, Lu, et al., 2017). With a PIC simulation model, Fu et al. (2017) suggested that the nonlinear coupling between two lower-band whistler mode waves could be a possible mechanism to excite oblique whistler mode waves. However, the pump whistler mode wave is usually required to have a finite WNA, since its electrostatic component is quite necessary in nonlinear coupling processes.

In this study, with a one-dimensional (1-D) PIC simulation model, we will investigate the nonlinear evolution of parallel counter-propagating whistler mode waves excited by anisotropic electrons, which are typically observed in the equatorial source region. In our simulations, after the linear phase of whistler mode instability, the electrostatic standing structures along the background magnetic field will appear, which are caused by the excited counter-propagating whistler mode waves. Moreover, we further find that whistler mode waves can be coupled with these electrostatic structures, driving high-k modes in this plasma system. This paper is organized as follows. The 1-D PIC simulation model and initial setup are presented in section 2, followed by the simulation results in section 3. At last, we will summarize the principle results and give some discussions in section 4.

2. 1-D PIC Simulation Model

For studying the nonlinear evolution of whistler mode waves within the equatorial source region, we have employed a 1-D PIC simulation model, which can solve three-dimensional velocities and electromagnetic fields but only allows spatial variations in the x direction (Gao, Ke, et al., 2017; Lu et al., 2004, 2010). This simulation model is performed in a magnetized, homogenous, and collisionless plasma with a periodic boundary. The background magnetic field is along the x axis, that is, $\mathbf{B_0} = B_0\hat{\mathbf{x}}$. This means the excited whistler mode waves will be strictly parallel or antiparallel propagating, which should be a typical situation within the equatorial source region. The simulation model consists of three plasma components representing cool electrons and protons (Maxwellian velocity distributions) and tenuous anisotropic hot electrons (bi-Maxwellian velocity distribution). Hereafter, subscripts "p," "c," and "h" refer to cool protons, cool electrons, and anisotropic hot electrons, respectively. For each species, there are on average 10,000 macroparticles in every cell. Their number densities are n_p, n_c, and n_h, respectively, and satisfy condition $n_p = n_c + n_h$. Because the proton gyrofrequency is much smaller than the frequency of whistler waves, protons are only treated as particles with infinite mass, which are simply assumed to be an immobile positively changed background.

All parameters in our simulations have been normalized. The magnetic fields and velocities are normalized by B_0 and V_{Ae} (where $V_{Ae} = B_0/\sqrt{\mu_0 n_0 m_e}$, μ_0 is the vacuum permeability, n_0, i.e., n_p, is the plasma density, and m_e is the mass of electron), while the units of space and time are V_{Ae}/Ω_e and the inverse of electron gyrofrequency Ω_e^{-1}. There are 2,048 grid cells in the simulation box, and the length of each cell is set as $\Delta x = 0.3V_{Ae}/\Omega_e$. If we assume the background magnetic field and plasma density to be B_0 = 80 nT and n_0 = 1 cm^{-3}, which are typical values at L-shell = 7 in the Earth's magnetosphere (Gao et al., 2014b; Li et al., 2009), then the ratio of the plasma frequency to electron gyrofrequency will be given as $\omega_{pe}/\Omega_e = 4$. The

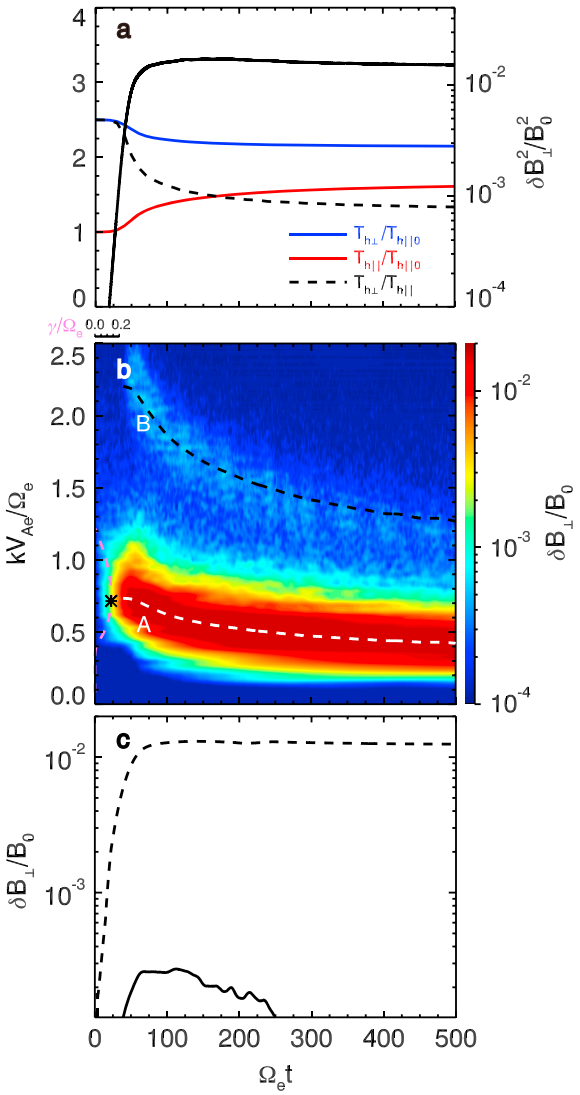

Figure 1. (a) Time history of the perpendicular temperature $T_{h\perp}/T_{h\|0}$ (blue solid line), parallel temperature $T_{h\|}/T_{h\|0}$ (red solid line), and temperature anisotropy $T_{h\perp}/T_{h\|}$ (black dashed line) of hot electrons and fluctuating magnetic fields $\delta B_\perp^2/B_0^2$ (black solid line); (b) The *k-t* spectrogram of fluctuating magnetic fields $\delta B_\perp/B_0$, which is obtained by performing the fast Fourier transform to $\delta B_\perp(x, t)/B_0$ only in the spatial space; (c) time evolution of magnetic amplitudes for bands A (dashed line) and B (solid line). In Figure 1b, the magenta dashed line represents the linear growth rates of whistler mode waves with asterisk marking the most unstable mode. The dominant wave number with the maximum power for band A is denoted by the white dashed line, while its third times given by the black dashed line.

thermal velocity for cool electrons is $v_c = 0.01V_{Ae}$. And the temperature of protons is the same as that of cool electrons, which means that their thermal velocity is $v_p = 2.3 \times 10^{-4}V_{Ae}$. The total simulation time is 500 Ω_e^{-1} with a time step $\Delta t = 0.025\Omega_e^{-1}$. Two simulation runs are performed in this study: case I with $n_h = n_0$, $v_{h\|} = 0.8V_{Ae}$, and $T_{h\perp}/T_{h\|} = 2.5$ (where $T_{h\perp}$ and $T_{h\|}$ are perpendicular and parallel temperatures of hot electrons, respectively) and case II with $n_h = 0.1n_0$, $v_{h\|} = 1.0V_{Ae}$, and $T_{h\perp}/T_{h\|} = 4.0$.

3. Simulation Results

Figure 1 gives an overview of case I, which displays (a) the time evolution of the perpendicular temperature $T_{h\perp}/T_{h\|0}$ (blue solid line), parallel temperature $T_{h\|}/T_{h\|0}$ (red solid line), temperature anisotropy $T_{h\perp}/T_{h\|}$ (black dashed line) of hot electrons, and fluctuating magnetic fields $\delta B_\perp^2/B_0^2$ (black solid line); (b) *k-t* magnetic spectrogram; and (c) time profiles of magnetic amplitudes for bands A (dashed line) and B (solid line). In Figure 1b, the magenta dashed line shows the linear growth rates of whistler mode waves as a function of wave numbers for the initial setup, which are calculated by using WHAMP model (https://github.com/irfu/whamp). The dominant wave number with the maximum power for band A is denoted by the white dashed line, while its third times given by the black dashed line. As shown in Figure 1a, the temperature anisotropy of hot electrons begins to decrease at ~$25\Omega_e^{-1}$, leading to the rapid enhancement of the fluctuating magnetic field energy. The fluctuating magnetic fields grow exponentially until ~$50\,\Omega_e^{-1}$ and saturate at ~$180\,\Omega_e^{-1}$ with the maximum amplitude as ~$1.7\times10^{-2}B_0^2$. Based on previous works, the anisotropic hot electrons are unstable to excite whistler mode waves, which will then scatter hot electrons to reduce their temperature anisotropy (Gary et al., 2000; Lu et al., 2010). The asterisk in Figure 1b marks the most unstable mode predicted by the linear theory with wave number ~$0.72V_{Ae}/\Omega_e$, which is consistent with the dominant wave number of band A at $25\Omega_e^{-1}$. Surprisingly, the *k-t* spectrogram of fluctuating magnetic fields exhibits a two-band structure, which includes the expected whistler mode waves with relatively smaller wave numbers (band A) and the high-*k* modes with relatively larger wave numbers (band B). We further find that the black dashed line quite follows the dominant wave number of band B, meaning the wave numbers of band B are nearly 3 times those of band A. Besides, the wave numbers of both bands are observed to drift to smaller values, which are similar to previous simulation results (Chen et al., 2017; Sydora et al., 2007). In Figure 1c, the magnetic amplitude of band A begins to increase from the very beginning, while the band B starts to grow just when band A has the sufficiently large magnetic amplitude. Moreover, the amplitude of band B is about 2 orders smaller than that of band A.

The dispersion relation of two bands is illustrated in Figure 2, where the black line gives the linear dispersion relation of whistler mode waves at $\Omega_e t = 100$ and the asterisks represent the dominant wave mode for each band. We can clearly find that bands A and B are propagating in both parallel ($k > 0$) and antiparallel ($k < 0$) directions. Here the magnetic fluctuations are decomposed into positive and negative helical parts following the method developed by Terasawa et al. (1986). Since whistler waves are right-hand polarized, then the positive and negative helical parts of fluctuating magnetic fields correspond to parallel and antiparallel propagating waves, respectively. The dominant mode of band A is located right on the linear dispersion

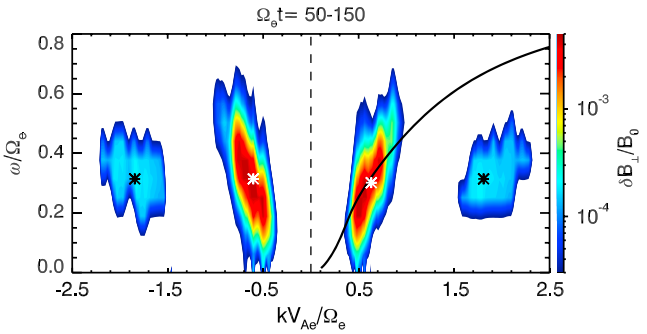

Figure 2. The dispersion relation of two bands during $\Omega_e t = 50 - 150$, where the black line represents the linear dispersion relation of whistler mode waves at $\Omega_e t = 100$. The white and black asterisks denote the dominant wave mode for bands A and B, respectively.

curve with $kV_{Ae}/\Omega_e \approx \pm 0.61$ and $\omega/\Omega_e \approx 0.31$, which indicates that band A belongs to counter-propagating whistler mode waves excited from anisotropic hot electrons. However, the dominant mode of band B is far away from the dispersion curve of whistler mode waves, suggesting the band B is not a normal mode in this plasma. Moreover, we further find the dominant wave number of band B is $\sim\pm 1.81 V_{Ae}/\Omega_e$, which is about 3 times that of band A, but the dominant wave modes of both bands nearly have the same frequency. Here the high-k modes in band B are generated through a series of wave-wave coupling processes during the nonlinear evolution of whistler mode waves, which will be shown in the following results.

Figure 3 displays the temporal evolution of (a) fluctuating magnetic fields $\delta B_y/B_0$ and (b) fluctuating electric fields $\delta E_x/V_{Ae}B_0$ along the x axis. Figure 3a shows that the disturbed magnetic fields begin to grow at $\sim 25\Omega_e^{-1}$ from the background noise level, which are whistler mode waves excited by anisotropic hot electrons. Moreover, whistler mode waves are observed to propagate in both parallel and antiparallel directions, which is supported by both the linear theory (Gary & Karimabadi, 2006; Kennel & Petschek, 1966; Omura et al., 2008; Scharer & Trivelpiece, 1967) and satellite observations (Li et al., 2013; Parrot et al., 2003; Santolik et al., 2005). Meanwhile, the wavelengths of whistler mode waves are found to increase with time, which is consistent with the drift of wave numbers shown in Figure 1b. For parallel propagating whistler mode waves, they are purely electromagnetic waves and should not have any electrostatic components (i.e., parallel electric fields). However, after $\sim 50\Omega_e^{-1}$, the parallel electric fields also show up at locations where the counter-propagating whistler mode waves meet (Figure 3b). We further find that these localized electric fluctuations are just electrostatic standing structures. Figure 4 shows the spatial profile of (a) fluctuating magnetic fields $\delta B_y/B_0$ and (b) fluctuating electric fields $\delta E_x/(V_{Ae}B_0)$ at $50\Omega_e^{-1}$. Since the whistler mode spectrum has a finite bandwidth (Figure 1b), the magnetic fields will experience strong modulation, leading to the formation of wave packets along the x axis (Figure 4). And the fluctuating electric fields are also strongly modulated in space, and their intensity is positively correlated with that of $\delta B_y/B_0$.

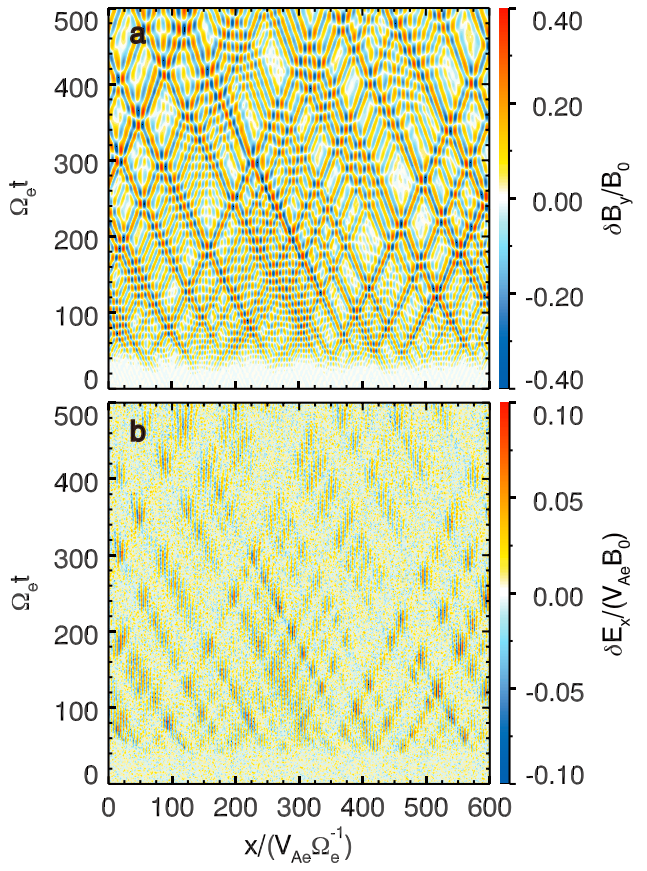

Figure 3. The temporal evolution of (a) fluctuating magnetic fields $\delta B_y/B_0$ and (b) fluctuating parallel electric fields $\delta E_x/V_{Ae}B_0$ along the x axis.

These electrostatic standing structures are further analyzed in Figure 5, which illustrates (a) the k-t spectrogram and (b) dispersion relation during $\Omega_e t = 50 - 100$ of parallel electric fields $\delta E_x/V_{Ae}B_0$. In Figure 5a, the black dashed line represents two times wave numbers of whistler mode waves in Figure 1b (white dashed line), which can well depict the time evolution of parallel electric fields. This means the dominant wave number of parallel electric fields is precisely twice that of whistler mode waves (band A). The maximum power is marked by an asterisk in Figure 5b, which is located at about $(1.25V_{Ae}/\Omega_e, 0\Omega_e)$. The dispersion relation has also confirmed that the fluctuating parallel electric fields should be electrostatic standing structures with twice wave numbers of counter-propagating whistler mode waves.

In our simulations, those electrostatic standing structures are generated due to the coupling between counter-propagating whistler mode waves, then they will be coupled with either the parallel or antiparallel propagating whistler mode waves to drive high-k modes in band B. Their phase coupling can be quantitatively measured by the bicoherence index, which is close to 1 when the involved three wave modes satisfy the resonant condition $\mathbf{k}_1 \pm \mathbf{k}_2 = \mathbf{k}_3$ and $\omega_1 \pm \omega_2 = \omega_3$ (van Milligen et al., 1995). Figure 6a gives the bicoherence index among the electrostatic standing structures (k_{Ex}) and counter-propagating

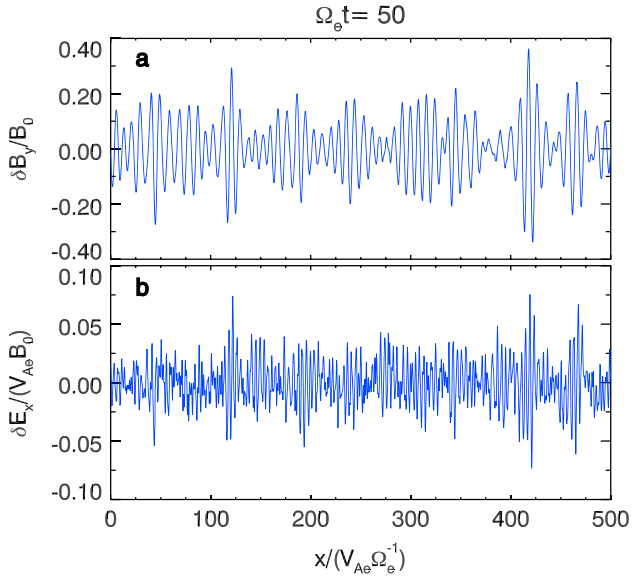

Figure 4. The spatial profile of (a) fluctuating magnetic fields $\delta B_y/B_0$ and (b) fluctuating parallel electric field $\delta E_x/V_{Ae}B_0$ along the x axis at $50\Omega_e^{-1}$.

whistler mode waves (k_{A+} and k_{A-}) during $\Omega_e t = 50 - 70$, while Figure 6 b displays the bicoherence index among the electrostatic standing structures (k_{Ex}), parallel propagating whistler mode waves (k_{A+}), and high-k modes in band B (k_{B+}) during $\Omega_e t = 50 - 70$. The bicoherence indices bc are defined as $\left|\left\langle B_y(k_{A+})B_y(k_{A-})E_x^*(k_{Ex})\right\rangle\right|^2 / \left\langle\left|B_y(k_{A+})B_y(k_{A-})\right|^2\right\rangle\left\langle\left|E_x^*(k_{Ex})\right|^2\right\rangle$ and $\left|\left\langle B_y(k_{A+})E_x(k_{Ex})B_y^*(k_{B+})\right\rangle\right|^2 / \left\langle\left|B_y(k_{A+})E_x(k_{Ex})\right|^2\right\rangle\left\langle\left|B_y^*(k_{B+})\right|^2\right\rangle$ (where $k_{Ex} = k_{A+} - k_{A-}$ and $k_{B+} = k_{Ex} + k_{A+}$ and the bracket $\langle\ldots\rangle$ represents a time average over the $20\ \Omega_e^{-1}$ interval), respectively. As displayed in Figure 6a, the maximum bc (black dashed circle) is just located at $k_{A+}V_{Ae}/\Omega_e \approx 0.74$, $k_{A-}V_{Ae}/\Omega_e \approx -0.74$, and $k_{Ex}V_{Ae}/\Omega_e \approx 1.48$, with $bc_{\max} \approx 0.55$, meaning there is a strong coupling process among two counter-propagating whistler mode waves and electrostatic standing structures with $k_{Ex} = k_{A+} - k_{A-} = 2k_{A+}$ satisfied. This phenomenon is similar to that reported in previous works about ion cyclotron waves (Guo, 2016; Mottez, 2012). Figure 6b shows a strong coupling among $k_{A+}V_{Ae}/\Omega_e \approx 0.73$, $k_{Ex}V_{Ae}/\Omega_e \approx 1.40$, and $k_{B+}V_{Ae}/\Omega_e \approx 2.13$, with $bc_{\max} \approx 0.52$ (white dashed circle). This indicates that the electrostatic standing structures can further be coupled with counter-propagating whistler mode waves to drive high-k modes, whose dominant wave number is about 3 times that of linearly excited whistler mode waves.

To produce a clearer banded spectrum, we choose an unrealistic initial setup in case I, that is, only the hot electrons are considered ($n_h = n_0$), but this will not affect the principle results shown here. Further, we have also performed another simulation run with a more realistic $n_h = 0.1n_0$ in the Earth's magnetosphere (Gao et al., 2014a), and its results are displayed in Figure 7. As shown in Figure 7a, although the high-k modes in band B are much weaker, we can still clearly find two bands in the plasma system, which is quite similar to the spectrum shown in Figure 1b. Moreover, the electrostatic standing structures are also significant, which are observed to have about twice wave numbers of excited whistler mode waves in band A (Figure 7b). The simulation results of case II indicate that the nonlinear coupling processes studied above should take place during the evolution of whistler mode waves within their equatorial source region in the magnetosphere.

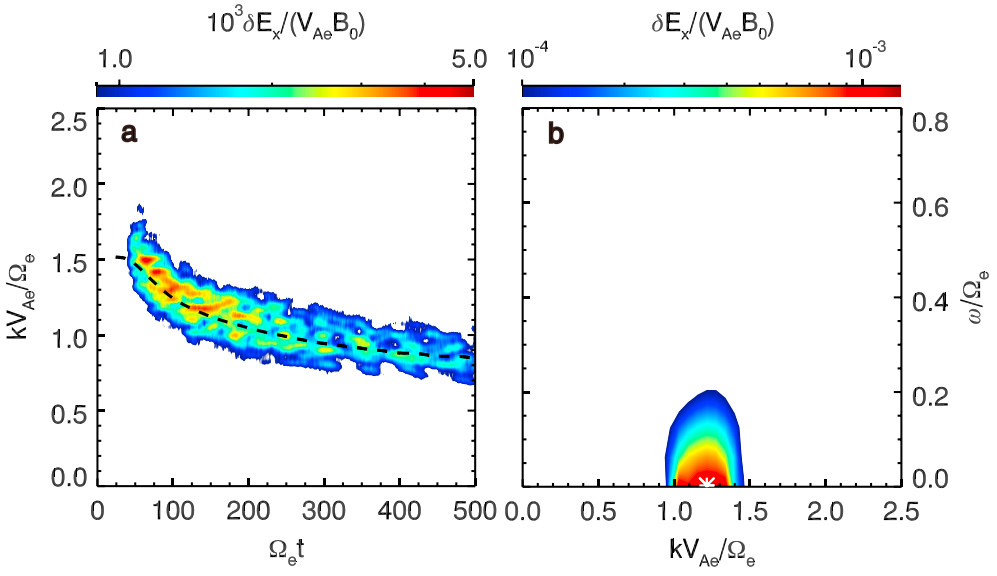

Figure 5. (a) The $k - t$ spectrogram and (b) dispersion relation of parallel electric fields $\delta E_x/V_{Ae}B_0$. The black dashed line in Figure 5a denotes 2 times wave numbers of whistler mode waves in Figure 1b (white dashed line).

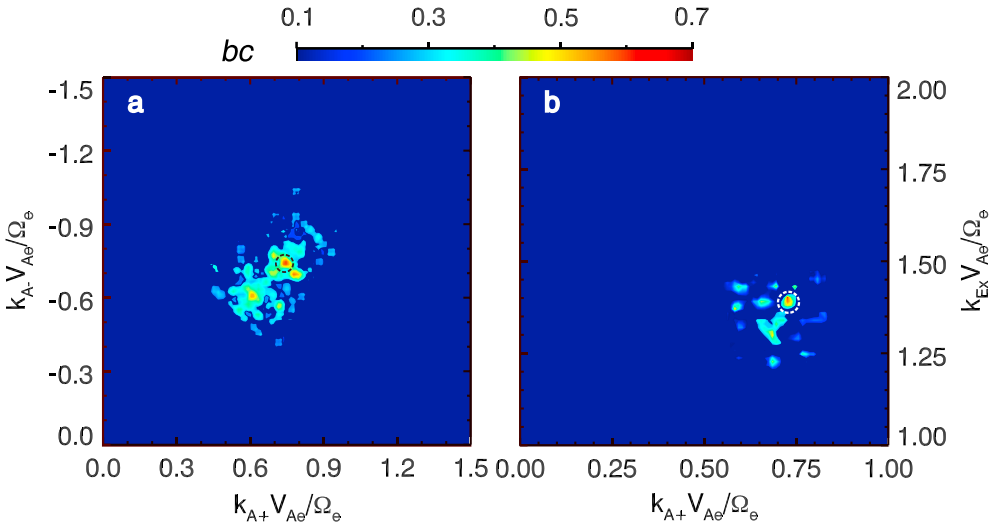

Figure 6. The bicoherence index (a) among the electrostatic standing structures (k_{Ex}) and counter-propagating whistler mode waves (k_{A+} and k_{A-}) and (b) among the electrostatic standing structures (k_{Ex}), parallel propagating whistler mode waves (k_{A+}), and the high-k modes in band B (k_{B+}) during $\Omega_e t = 50 - 70$. The maximum bc is pointed out by the black and white dashed circles in Figures 6a and 6b, respectively.

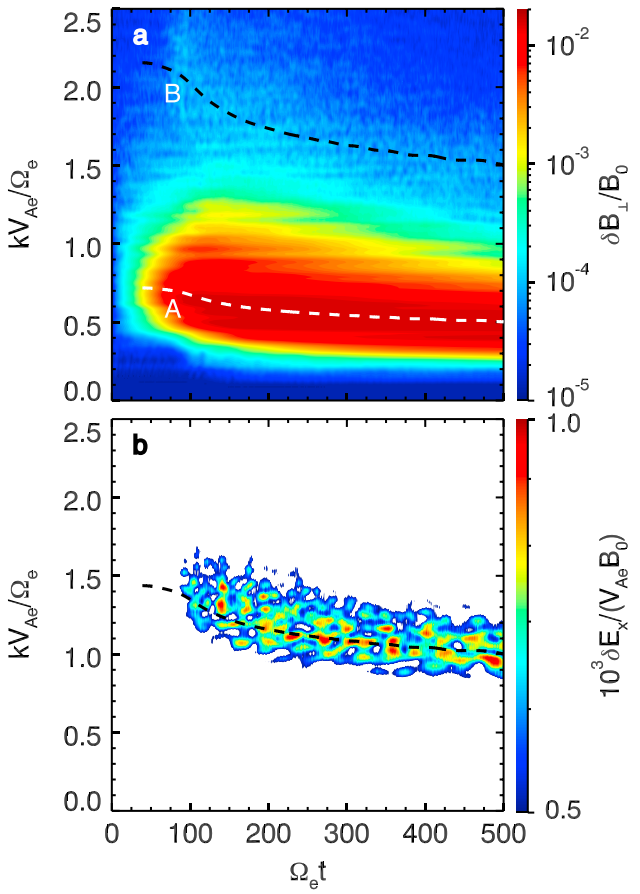

Figure 7. The k-t spectrum of (a) fluctuating magnetic fields $\delta B_\perp/B_0$ and (b) parallel fluctuating electric fields $\delta E_x/V_{Ae}B_0$ for case II with the same format as Figures 1b and 5a, respectively.

4. Conclusions and Discussion

With a 1-D PIC simulation model, we have studied the nonlinear evolution of parallel counter-propagating whistler mode waves excited by anisotropic electrons within the equatorial source region. In our simulations, after the linear phase of whistler mode instability, the strong electrostatic standing structures along the background magnetic field will appear, which are caused by the couplings between excited counter-propagating whistler mode waves. The wave numbers of electrostatic standing structures are about twice those of whistler mode waves generated by anisotropic hot electrons. Moreover, these electrostatic standing structures can further be coupled with either parallel or anti-parallel propagating whistler mode waves to drive high-k modes in this plasma system, and these high-k modes are not normal modes in this plasma system. Compared with excited whistler mode waves, these high-k modes typically have 3 times wave number, same frequency, and about 2 orders of magnitude smaller amplitude.

Nonlinear wave-wave interactions related to whistler mode waves are becoming a hot topic, since their formed fine spectral structures have a significant influence on wave-particles interactions in the Earth's magnetosphere. The previous works have already demonstrated that whistler mode waves with finite WNAs can not only drive multiband chorus waves (Chen et al., 2017; Gao, Lu, et al., 2016; Gao, Ke, et al., 2017) but also be coupled with each other to drive oblique waves (Fu et al., 2017; Gao, Lu, et al., 2017). However, within the equatorial source region, whistler mode waves usually have negligible WNAs, which are previously expected to be stable. Besides, those whistler mode waves are also detected to propagate both northward and southward (Li et al., 2013; Parrot et al., 2003; Santolik et al., 2005). Based on our simulation results, the strong electrostatic standing structures along the background magnetic field can be formed (Figures 5 and 7), resulting from the coupling between excited

counter-propagating whistler mode waves (Figures 3 and 6). Moreover, these electrostatic standing structures can further be coupled with whistler mode waves to excite the high-*k* modes (Figures 1 and 7). The wave number of the high-*k* mode is triple that of the whistler wave, while their frequencies are nearly the same. Meanwhile, the frequency of electrostatic structures is almost zero. Therefore, both the high-*k* mode and electrostatic structures cannot be identified in the time-frequency spectrogram from single-satellite observations. The most promising way to identify them is through the wave number analysis, which then requires the multiple-satellite observations. The latest MMS mission (Burch et al., 2016), consisting of four nearby probes, may be more suitable for studying this nonlinear process, but this is beyond the scope of this paper and left to a separate study. Meanwhile, how these high-*k* modes and electrostatic standing structures interact with electrons is also worthy of further investigation. As a summary, our results may provide a new insight into the nonlinear evolution of whistler mode waves within their equatorial source regions in the Earth's magnetosphere.

Acknowledgments
This research was supported by the NSFC grants 41774151, 41604128, 41631071, and 41331067; the Youth Innovation Promotion Association of Chinese Academy of Sciences (2016395); the Specialized Research Fund for State Key Laboratories; and the Key Research Program of Frontier Sciences, CAS (QYZDJ-SSW-DQC010). The simulation data used in our paper can be accessed online (https://pan.baidu.com/s/1pLmQYeR).

References

Burch, J. L., Moore, T. E., Torbert, R. B., & Giles, B. L. (2016). Magnetospheric multiscale overview and science objectives. *Space Science Reviews*, *199*(1-4), 5–21. https://doi.org/10.1007/s11214-015-0164-9

Burtis, W. J., & Helliwell, R. A. (1969). Banded chorus a new type of VLF radiation observed in the magnetosphere by OGO 1 and OGO 3. *Journal of Geophysical Research*, *74*(11), 3002–3010. https://doi.org/10.1029/JA074i011p03002

Burton, R. K., & Holzer, R. E. (1974). The origin and propagation of chorus in the outer magnetosphere. *Journal of Geophysical Research*, *79*(7), 1014–1023. https://doi.org/10.1029/JA079i007p01014

Chen, H. Y., Gao, X. L., Lu, Q. M., Ke, Y. G., & Wang, S. (2017). Lower band cascade of whistler waves excited by anisotropic hot electrons: One-dimensional PIC simulations. *Journal of Geophysical Research: Space Physics*, *122*, 10,448–10,457. https://doi.org/10.1002/2017JA024513

Fu, X., Cowee, M. M., Friedel, R. H., Funsten, H. O., Gary, S. P., Hospodarsky, G. B., et al. (2014). Whistler anisotropy instabilities as the source of banded chorus: Van Allen Probes observations and particle-in-cell simulations. *Journal of Geophysical Research: Space Physics*, *119*, 8288–8298. https://doi.org/10.1002/2014JA020364

Fu, X. R., Gary, S. P., Reeves, G. D., Winske, D., & Woodroffe, J. R. (2017). Generation of highly oblique lower-band chorus via nonlinear three-wave resonance. *Geophysical Research Letters*, *44*, 9532–9538. https://doi.org/10.1002/2017GL074411

Gao, X. L., Li, W., Thorne, R. M., Bortnik, J., Angelopoulos, V., Lu, Q. M., et al. (2014a). New evidence for generation mechanisms of discrete and hiss-like whistler mode waves. *Geophysical Research Letters*, *41*, 4805–4811. https://doi.org/10.1002/2014GL060707

Gao, X., Li, W., Thorne, R. M., Bortnik, J., Angelopoulos, V., Lu, Q., et al. (2014b). Statistical results describing the bandwidth and coherence coefficient of whistler mode waves using THEMIS waveform data. *Journal of Geophysical Research: Space Physics*, *119*, 8992–9003. https://doi.org/10.1002/2014JA020158

Gao, X. L., Lu, Q. M., Bortnik, J., Li, W., Chen, L. J., & Wang, S. (2016). Generation of multiband chorus by lower band cascade in the Earth's magnetosphere. *Geophysical Research Letters*, *43*, 2343–2350. https://doi.org/10.1002/2016GL068313

Gao, X. L., Mourenas, D., Li, W., Artemyev, A. V., Lu, Q. M., Tao, X., & Wang, S. (2016). Observational evidence of generation mechanisms for very oblique lower band chorus using THEMIS waveform data. *Journal of Geophysical Research: Space Physics*, *121*, 6732–6748. https://doi.org/10.1002/2016JA022915

Gao, X. L., Ke, Y. G., Lu, Q. M., Chen, L. J., & Wang, S. (2017). Generation of multiband chorus in the Earth's magnetosphere: 1-D PIC simulation. *Geophysical Research Letters*, *44*, 618–624. https://doi.org/10.1002/2016GL072251

Gao, X. L., Lu, Q. M., & Wang, S. (2017). First report of resonant interactions between whistler mode waves in the Earth's magnetosphere. *Geophysical Research Letters*, *44*, 5269–5275. https://doi.org/10.1002/2017GL073829

Gary, S. P., & Karimabadi, H. (2006). Linear theory of electron temperature anisotropy instabilities: Whistler, mirror, and Weibel. *Journal of Geophysical Research*, *111*, A11224. https://doi.org/10.1029/2006JA011764

Gary, S. P., Winske, D., & Hesse, M. (2000). Electron temperature anisotropy instabilities: Computer simulations. *Journal of Geophysical Research*, *105*(A5), 10,751–10,759. https://doi.org/10.1029/1999JA000322

Guo, J. (2016). The generation and evolution of multi-band EMIC waves in the magnetosphere: Hybrid simulations. *Advances in Space Research*, *58*(11), 2460–2468. https://doi.org/10.1016/j.asr.2016.08.012

Helliwell, R. A. (1967). A theory of discrete emissions from the magnetosphere. *Journal of Geophysical Research*, *72*(19), 4773–4790. https://doi.org/10.1029/JZ072i019p04773

Horne, R. B., & Thorne, R. M. (1998). Potential waves for relativistic electron scattering and stochastic acceleration during magnetic storms. *Geophysical Research Letters*, *25*(15), 3011–3014. https://doi.org/10.1029/98GL01002

Horne, R. B., Thorne, R. M., Meredith, N. P., & Anderson, R. R. (2003). Diffuse auroral electron scattering by electron cyclotron harmonic and whistler mode waves during an isolated substorm. *Journal of Geophysical Research*, *108*(A7), 1290. https://doi.org/10.1029/2002JA009736

Ke, Y. G., Gao, X., Lu, Q., Wang, X., & Wang, S. (2017). Generation of rising-tone chorus in a two-dimensional mirror field by using the general curvilinear PIC code. *Journal of Geophysical Research: Space Physics*, *122*, 8154–8165. https://doi.org/10.1002/2017JA024178

Kennel, C. F., & Petschek, H. E. (1966). Limit on stably trapped particle fluxes. *Journal of Geophysical Research*, *71*(1), 1–28. https://doi.org/10.1029/JZ071i001p00001

LeDocq, M. J., Gurnett, D. A., & Hospodarsky, G. B. (1998). Chorus source locations from VLF Poynting flux measurements with the Polar spacecraft. *Geophysical Research Letters*, *25*(21), 4063–4066. https://doi.org/10.1029/1998GL900071

Li, W., Thorne, R. M., Angelopoulos, V., Bortnik, J., Cully, C. M., Ni, B., et al. (2009). Global distribution of whistler-mode chorus waves observed on the THEMIS spacecraft. *Geophysical Research Letters*, *36*, L09104. https://doi.org/10.1029/2009GL037595

Li, W., Thorne, R. M., Nishimura, Y., Bortnik, J., Angelopoulos, V., McFadden, J. P., et al. (2010). THEMIS analysis of observed equatorial electron distributions responsible for the chorus excitation. *Journal of Geophysical Research*, *115*, A00F11. https://doi.org/10.1029/2009JA014845

Li, W., Bortnik, J., Thorne, R. M., & Angelopoulos, V. (2011). Global distribution of wave amplitudes and wave normal angles of chorus waves using THEMIS wave observations. *Journal of Geophysical Research*, *116*, A12205. https://doi.org/10.1029/2011JA017035

Li, W., Thorne, R. M., Bortnik, J., Tao, X., & Angelopoulos, V. (2012). Characteristics of hiss-like and discrete whistler-mode emissions. *Geophysical Research Letters*, *39*, L18106. https://doi.org/10.1029/2012GL053206

Li, W., Bortnik, J., Thorne, R. M., Cully, C. M., Chen, L., Angelopoulos, V., et al. (2013). Characteristics of the Poynting flux and wave normal vectors of whistler-mode waves observed on THEMIS. *Journal of Geophysical Research: Space Physics*, *118*, 1461–1471. https://doi.org/10.1002/jgra.50176

Lorentzen, K. R., Blake, J. B., Inan, U. S., & Bortnik, J. (2001). Observations of relativistic electron microbursts in association with VLF chorus. *Journal of Geophysical Research*, *106*(A4), 6017–6027. https://doi.org/10.1029/2000JA003018

Lu, Q. M., Wang, L. Q., Zhou, Y., & Wang, S. (2004). Electromagnetic instabilities excited by electron temperature anisotropy. *Chinese Physics Letters*, *21*(8), 1518–1521. https://doi.org/10.1088/0256-307X/21/8/029

Lu, Q. M., Zhou, L. H., & Wang, S. (2010). Particle-in-cell simulations of whistler waves excited by an electron kappa distribution in space plasma. *Journal of Geophysical Research*, *115*, A02213. https://doi.org/10.1029/2009JA014580

Meredith, N. P., Horne, R. B., & Anderson, R. R. (2001). Substorm dependence of chorus amplitudes: Implications for the acceleration of electrons to relativistic energies. *Journal of Geophysical Research*, *106*(A7), 13,165–13,178. https://doi.org/10.1029/2000JA900156

Mottez, F. (2012). Non-propagating electric and density structures formed through non-linear interaction of Alfvén waves. *Annales de Geophysique*, *30*(1), 81–95, https://doi.org/10.5194/angeo-30-81-2012.

Ni, B., Thorne, R. M., Shprits, Y. Y., & Bortnik, J. (2008). Resonant scattering of plasma sheet electrons by whistler-mode chorus: Contribution to diffuse auroral precipitation. *Geophysical Research Letters*, *35*, L11106. https://doi.org/10.1029/2008GL034032

Ni, B., Thorne, R. M., Meredith, N. P., Shprits, Y. Y., & Horne, R. B. (2011). Diffuse auroral scattering by whistler mode chorus waves: Dependence on wave normal angle distribution. *Journal of Geophysical Research*, *116*, A10207. https://doi.org/10.1029/2011JA016517

Nishimura, Y., Bortnik, J., Li, W., Thorne, R. M., Ni, B., Lyons, L. R., et al. (2013). Structures of dayside whistler-mode waves deduced from conjugate diffuse aurora. *Journal of Geophysical Research: Space Physics*, *118*, 664–673. https://doi.org/10.1029/2012JA018242

Omura, Y., Katoh, Y., & Summers, D. (2008). Theory and simulation of the generation of whistler-mode chorus. *Journal of Geophysical Research*, *113*, A04223. https://doi.org/10.1029/2007JA012622

Parrot, M., Santolík, O., Cornilleau-Wehrlin, N., Maksimovic, M., & Harvery, C. C. (2003). Source location of chorus emissions observed by Cluster. *Annales de Geophysique*, *21*(2), 473–480. https://doi.org/10.5194/angeo-21-473-2003

Santolík, O., Gurnett, D. A., Pickett, J. S., Parrot, M., & Cornilleau-Wehrlin, N. (2003). Spatio-temporal structure of storm-time chorus. *Journal of Geophysical Research*, *108*(A7), 1278. https://doi.org/10.1029/2002JA009791

Santolik, O., Gurnett, D. A., Pickett, J. S., Parrot, M., & Cornilleau-Wehirlin, N. (2005). Central position of the source region of storm-time chorus. *Planetary and Space Science*, *53*(1-3), 299–305. https://doi.org/10.1016/j.pss.2004.09.056

Scharer, J. E., & Trivelpiece, A. W. (1967). Cyclotron wave instabilities in a plasma. *Physics of Fluids*, *10*(3), 591. https://doi.org/10.1063/1.1762153

Summers, D., Thorne, R. M., & Xiao, F. L. (1998). Relativistic theory of wave-particle resonant diffusion with application to electron acceleration in the magnetosphere. *Journal of Geophysical Research*, *103*(A9), 20,487–20,500. https://doi.org/10.1029/98JA01740

Sydora, R. D., Sauer, K., & Silin, I. (2007). Coherent whistler waves and oscillation formation: Kinetic simulations. *Geophysical Research Letters*, *34*, L22105. https://doi.org/10.1029/2007GL031839

Terasawa, T., Hoshino, M., Sakai, J. I., & Hada, T. (1986). *Journal of Geophysical Research*, *91*(A4), 4171–4187. https://doi.org/10.1029/JA09liA04p04171

Thorne, R. M., Ni, B., Tao, X., Horne, R. B., & Meredith, N. P. (2010). Scattering by chorus waves as the dominant cause of diffuse auroral precipitation. *Nature*, *467*(7318), 943–946. https://doi.org/10.1038/nature09467

Thorne, R. M., Li, W., Ni, B., Ma, Q., Bortnik, J., Chen, L., et al. (2013). Rapid local acceleration of relativistic radiation-belt electrons by magnetospheric chorus. *Nature*, *504*(7480), 411–414. https://doi.org/10.1038/nature12889

Tsurutani, B. T., & Smith, E. J. (1974). Postmidnight chorus: A substorm phenomenon. *Journal of Geophysical Research*, *79*(1), 118–127. https://doi.org/10.1029/JA079i001p00118

van Milligen, B. P., Sanchez, E., Estrada, T., Hidalgo, C., Branas, B., Carreras, B., & Garcia, L. (1995). Wavelet bicoherence: A new turbulence analysis tool. *Physics of Plasmas*, *2*(8), 3017–3032. https://doi.org/10.1063/1.871199

Xiao, F., et al. (2014). Chorus acceleration of radiation belt relativistic electrons during March 2013 geomagnetic storm. *Journal of Geophysical Research*, *119*, 3325–3332. https://doi.org/10.1002/2014JA019822